Justifying the thin-crystal approximation in spontaneous parametric down-conversion for collinear phase matching

Baghdasar Baghdasaryan,[1,2,3,*] Fabian Steinlechner,[3,4] and Stephan Fritzsche[1,2,4]

[1]*Theoretisch-Physikalisches Institut, Friedrich-Schiller-Universität Jena, D-07743 Jena, Germany*

[2]*Helmholtz-Institut Jena, D-07743 Jena, Germany*

[3]*Fraunhofer Institute for Applied Optics and Precision Engineering IOF, Albert-Einstein-Strasse 7, 07745 Jena, Germany*

[4]*Abbe Center of Photonics, Friedrich-Schiller-University Jena, Albert-Einstein-Strasse 6, 07745 Jena, Germany*

(Received 10 April 2021; accepted 1 June 2021; published 15 June 2021)

Spatially engineered photons from spontaneous parametric down-conversion (SPDC) are a valuable tool for studying and applying photonic entanglement. An advantage of SPDC is that simple expressions for the two-photon state can be obtained using justified approximations. In particular, the thin-crystal approximation has often been invoked in the engineering of high-dimensional entangled states. Knowledge of the conditions under which the thin-crystal approximation remains valid is essential for the realization of experimental setups. We provide a quantitative guideline on the validity of the thin-crystal approximation in calculating the two-photon spatial state. In particular, we show that the applicability of this regime is related to the focusing parameter $\overline{w}_p = w_p/\sqrt{\lambda_p L}$, where w_p and λ_p are the beam waist and wavelength of the pump beam, respectively, and L is the length of the nonlinear crystal. Additionally, the validity of the thin-crystal regime is investigated concerning the size of a subspace in the Laguerre Gaussian basis, into which the two-photon state can be projected in a given experiment.

DOI: 10.1103/PhysRevA.103.063508

Spontaneous parametric down-conversion (SPDC) is a nonlinear (optical) process that converts high-energy photons by a nonlinear crystal into pairs of entangled photons, also known as *signal* and *idler*. In general, these pairs of photons can be entangled in either time bins [1–4], polarization [5–8], path [9], or in the spatial degree of freedom [10–14] depending on the interplay between pump field and interaction geometry. The efficiency of the photon-pair generation hereby depends on the fulfillment of the wave vector conservation, $\delta \boldsymbol{k} \approx 0$, also called phase-matching condition.

The phase-matching or momentum conservation condition can be achieved for specific target emission directions and wavelengths by techniques such as quasi-phase-matching or birefringent phase-matching [15]. Thereby one distinguishes between type-I [16] and type-II [17,18] interactions, depending on the polarization of interacting fields (see Fig. 1).

The characteristics of SPDC pairs can also be well explained theoretically [19–21]. The state of a photon pair also called the two-photon state, is derived from the second-order perturbation theory. The third order of the perturbation theory gives rise to four photons generation, which is an unlikely process and can be neglected. Here, we consider particular experimental setups of SPDC, namely collinear and paraxial geometries. The collinear geometries refer to the situation where the pump, signal, and idler beams propagate nearly in the same direction. If the angles between these beams is in the range $0 - 5^\circ$, the collinear regime could be still assumed well fulfilled. Note that noncollinear geometries cause a violation of the conservation of orbital angular momentum in SPDC [22]. Paraxial geometries, in turn, assume that the transverse component of the momentum vector is much smaller than the longitudinal component for each of the three beams. Any research under these conditions will still be of great interest since most experiments are performed in these regimes. For simplicity, we will also assume that the refractive indices at the pump, signal, and idler wavelengths are equal $n_p \approx n_s \approx n_i$. For instance, this is a good approximation for β-barium borate (BBO) crystal in a large range of wavelengths $\lambda_p = 200 - 1000$ nm [23].

Experimentalists also often use approximations to model experimental setups. An often-utilized approximation is the assumption of a narrow-band spectrum for the signal and idler beams. Usually, signal and idler beams are not spectrally pure. They possess anticorrelation over many frequency modes, which may preclude any observation of multi-photon interference. This is, in turn, catastrophic for entanglement-swapping protocol [24]. For this paper, we consider the frequency state independent of the spatial state, i.e., there are no correlations between spectral and spatial state. Experimentally this scenario is readily obtained by placement of interference filters in front of the detectors.

The next approximation, which has been widely used in theoretical [22,25] and experimental [26–30] investigations, is the thin-crystal approximation: If the crystal length is much smaller than the Rayleigh range of the pump beam, $L \ll z_R$, the two-photon state is independent of the crystal features. Moreover, in this thin-crystal approximation, the two-photon state can be shaped by adjusting the pump beam. This property has been used previously in order to engineer high-dimensional entangled states [31–35].

*baghdasar.baghdasaryan@uni-jena.de

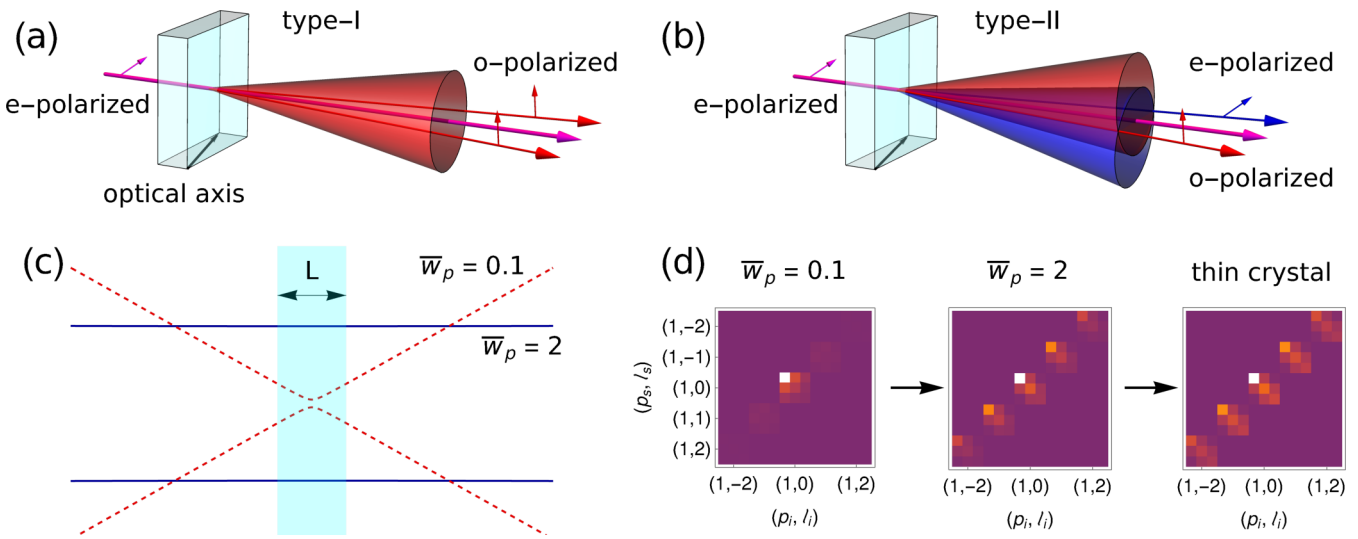

FIG. 1. Refractive index of birefringent materials depends on the polarization and propagation direction of the incident light. Consider the plane formed by the optic axis of the crystal and the propagation direction of the incident beam. The light is then called "ordinary polarized" (o-polarized) if its polarization direction is perpendicular to that plane. It is called "extraordinary polarized" (e-polarized) if its polarization direction is parallel to the plane mentioned above. Subfigure (a) shows the type-I phase matching. The signal and idler beams form a single cone and are both polarized in the ordinary direction. In contrast, the pump beam is polarized in an extraordinary direction. (b) In type-II phase matching, the pump beam is again polarized in an extraordinary direction. However, here the signal and idler beams have different polarization and form two cones. Note that the polarization states of signal and idler photons are indistinguishable in the intersection points of two cones. Furthermore, in collinear geometries, the opening angle of cones is very small, and the beams propagate almost in the same direction. Subfigures (a) and (b) do not represent the collinear geometries, but they are just for the illustrations of general type-I and type-II phase matching geometries. The angle between signal (idler) and pump beams in collinear experimental setups can be up to 5°. Paraxial geometries mean that the deviation from propagation directions is negligible, i.e., the transverse momentum of the beam is much smaller than the longitudinal component. Subfigure (c) indicates the experimental scenario, where two pump beams with different focusing parameters $\overline{w}_p = 0.1$ (dashed curves) and $\overline{w}_p = 2$ (solid curves) are focused in the middle of a crystal of length L. We see that the curvature of the beam with large $\overline{w}_p$ does not change during the propagation in the crystal. Hence, the change of the pump beam focusing plane would cause no change in the two-photon state. Subfigure (d) show the mode distribution of two-photon state in LG basis for different focusing parameters. The plots have been calculated with the amplitudes of the thick-crystal regime $C^{\ell_s,\ell_i}_{p_s,p_i}$ in the subspace $p_{s,i} = 0$, 1 and $\ell_{s,i} = -2$, -1, 0, 1, 2. The larger $\overline{w}_p$ is, the better is the thin-crystal approximation justified. Moreover, the deviation between the same modes from the thick- and thin-crystal regimes increases with the mode number $2p + \ell$.

The accessibility of the investigations in the thin-crystal or narrow-band regimes depends on the validity of these approximations. Therefore, the determination of the limits of both regimes attaches importance. Here, we will investigate only the thin-crystal approximation assuming that the narrow-band regime is valid. The investigation of the limits of the narrow-band regime remains still an exciting topic for future studies.

Previously, the thin-crystal regime has been investigated by Ramírez *et al*. [36]. For a given pump beam radius w_p, they introduced a critical length of the crystal L_c, with the following property: If the crystal length is smaller than the critical length $L < L_c$, the crystal properties are suppressed, and the pump beam features determine the angular spectrum of generated photons. However, a quantitative discussion of the two-photon mode distribution depending on the validity of the thin-crystal approximation is still missing. Here, we will analyze how the Rayleigh range of the pump beam or the crystal length should be chosen in order to reach a good fulfillment of the thin-crystal regime.

To analyze the thin-crystal approximation, we need first to construct the spatial structure of the two-photon state for the thick and thin-crystal regimes. Secondly, we should define a quantity to determine the distance between these two states.

Let us start with the expression of the two-photon state in the thick-crystal regime [20,28],

$$|\Psi_{\rm SPDC}\rangle = A \iint d\boldsymbol{q}_s \, d\boldsymbol{q}_i \, \Phi(\boldsymbol{q}_s, \boldsymbol{q}_i) \, \hat{a}^\dagger_s(\boldsymbol{q}_s) \, \hat{a}^\dagger_i(\boldsymbol{q}_i) \, |00\rangle \,, \quad (1)$$

where A is a normalization factor, $|00\rangle$ is the vacuum state, $\boldsymbol{q}_{s,i}$ are the transverse components of the signal and idler wave vectors, and $\hat{a}^\dagger_{s,i}(\boldsymbol{q}_{s,i})$ are the creation operators of the signal and idler modes. The form of the two-photon state (1) refers to creating two photons from the vacuum state, where all possible transverse momenta of signal and idler photons are considered through the integration in the momentum space. The so-called two-photon mode function $\Phi(\boldsymbol{q}_s, \boldsymbol{q}_i)$ describes the coupling between the wave vectors of the pump, signal, and idler beams. It consists of the product of the angular spectrum of the pump beam and the phase-matching function [37]:

$$\Phi(\boldsymbol{q}_s, \boldsymbol{q}_i) = \overbrace{\mathrm{V}(\boldsymbol{q}_s + \boldsymbol{q}_i)}^{\text{Pump}} \underbrace{\operatorname{sinc}\left(\frac{L|\boldsymbol{q}_s - \boldsymbol{q}_i|^2}{4k_p}\right)}_{\text{Phase Matching}} . \quad (2)$$

This expression refers to an experimental scenario, where a pump beam with a wave vector $k_p = 2z_R/w_p^2$ propagates along the z axis and interacts with the nonlinear crystal of length L placed in the $x-y$ plane at $z = -L/2$ (see Fig. 1). Despite the simple form of the two-photon mode function (2), it describes many experimental results very accurately [38–41].

Let us now consider the condition of the thin-crystal approximation $L \ll z_R$. Under this condition, the argument of the sinc function becomes very small. Consequently, the function itself can be approximated to one. Next, we replace all functions from Eq. (1) with their Fourier transform and execute the integration over $\boldsymbol{q}_s$ and $\boldsymbol{q}_i$. It is then easy to show that the four-dimensional integration in momentum-space can be replaced by a mathematically more straightforward two-dimensional integral in real space [20,42],

$$|\tilde{\Psi}_{\mathrm{SPDC}}\rangle = \int d\boldsymbol{r}_\perp \mathrm{V}(\boldsymbol{r}_\perp)\, \hat{a}_s^\dagger(\boldsymbol{r}_\perp)\, \hat{a}_i^\dagger(\boldsymbol{r}_\perp)\, |00\rangle\,, \tag{3}$$

where the *tilde* refers to the thin-crystal regime, $\boldsymbol{r}_\perp$ is the radial coordinate with regard to the beam axis, and $\mathrm{V}(\boldsymbol{r}_\perp)$ is the spatial distribution of the pump beam at the input face of the crystal. The investigation of the transition from the thick-crystal (1) to the thin-crystal regime (3) is the main topic of this paper.

As we mentioned before, here we are interested in the spatial structure of the two-photon state that can be expressed as a mode decomposition in terms of Laguerre Gaussian (LG) modes $|p,\ell\rangle = \int d\boldsymbol{q}\, \mathrm{LG}_{p,\ell}(\boldsymbol{q})\, \hat{a}^\dagger(\boldsymbol{q})\, |0\rangle$ [25,37,42],

$$|\Psi_{\mathrm{SPDC}}\rangle = \sum_{p_s,p_i=0}^{\infty} \sum_{\ell_s,\ell_i=-\infty}^{\infty} C_{p_s,p_i}^{\ell_s,\ell_i}\, |p_s\ell_s; p_i\ell_i\rangle\,, \tag{4}$$

where $p_{s,i}$ and $\ell_{s,i}$ are the discrete mode numbers of signal and idler photons, also called the radial and orbital angular momentum numbers [43]. The expansion coefficients in the thick- and thin-crystal regimes are given respectively by

$$\begin{aligned} C_{p_s,p_i}^{\ell_s,\ell_i} &= \iint \langle p_s\ell_s; p_i\ell_i|\Psi_{\mathrm{SPDC}}\rangle \\ &= \iint d\boldsymbol{q}_s\, d\boldsymbol{q}_i\, \Phi(\boldsymbol{q}_s,\boldsymbol{q}_i)\big[\mathrm{LG}_{p_s,\ell_s}(\boldsymbol{q}_s)\big]^*\big[\mathrm{LG}_{p_i,\ell_i}(\boldsymbol{q}_i)\big]^*, \end{aligned} \tag{5}$$

$$\begin{aligned} \tilde{C}_{p_s,p_i}^{\ell_s,\ell_i} &= \iint \langle p_s\ell_s; p_i\ell_i|\tilde{\Psi}_{\mathrm{SPDC}}\rangle \\ &= \int d\boldsymbol{r}_\perp \mathrm{V}(\boldsymbol{r}_\perp)\left[\mathrm{LG}_{p_s,\ell_s}(\boldsymbol{r}_\perp)\right]^*\left[\mathrm{LG}_{p_i,\ell_i}(\boldsymbol{r}_\perp)\right]^*. \end{aligned} \tag{6}$$

If the sums run over all possible p and ℓ, the state (4) is independent of the choice of the basis. On the other hand, the signal-to-noise ratio increases with selected values of p and ℓ, leading to difficulties in detecting high modes. Therefore, most of the spatial correlation experiments are performed in small subspaces. Mathematically *subspace* means that the summation in Eq. (4) is restricted to a particular range of p and ℓ. Therefore, we will discuss the validity of the thin-crystal regime also for in experiments available spatial subspace. As a pump laser, we will consider a Gaussian beam, as it is the most used pump beam in SPDC experiments:

$$\mathrm{V}(\boldsymbol{q}_s+\boldsymbol{q}_i) = \frac{w_p}{\sqrt{2\pi}} \exp\left(-\frac{w_p^2}{4}|\boldsymbol{q}_s+\boldsymbol{q}_i|^2\right).$$

The two-photon states are then constructed using Eq. (4), where $C_{p_s,p_i}^{\ell_s,\ell_i}$ are calculated numerically [25], and $\tilde{C}_{p_s,p_i}^{\ell_s,\ell_i}$ are received from an analytical expression [32,42].

We can now construct the states from the thick- and thin-crystal regimes. However, we are still missing the quantity, which should determine the similarity of these two quantum states. For this goal, we can use an appropriate distance measure such as *fidelity* or *trace distance*. For the states from Eqs. (1) and (3), the trace distance is then given by [44]

$$D = \sqrt{1 - |\langle\tilde{\Psi}_{\mathrm{SPDC}}|\Psi_{\mathrm{SPDC}}\rangle|^2}, \tag{7}$$

where the scalar product $|\langle\tilde{\Psi}_{\mathrm{SPDC}}|\Psi_{\mathrm{SPDC}}\rangle|$ is the fidelity of these two states. In general, if two quantum states are identical, the scalar product between them is equal to one, and consequently, the trace distance $D = 0$. However, if the states are perpendicular, the scalar product is equal to zero, representing the trace distance $D = 1$. In the following, we analyze the dependence of the trace distance on crystal and pump beam parameters and find conditions that minimize D. This will determine under which experimental conditions the thin-crystal approximation has very good predictive behavior.

The normalized amplitudes $C_{p_s,p_i}^{\ell_s,\ell_i}$ in the LG-mode decomposition can be shown to depend only on the dimensionless focusing parameter $\overline{w}_p$ defined by [37]

$$\overline{w}_p = \frac{w_p}{\sqrt{\lambda_p L}} = \sqrt{\frac{z_R}{\pi\, n_p\, L}}, \tag{8}$$

where n_p is the refractive index that the pump beam of wavelength λ_p experiences in the crystal. Note, that we chose for the LG waists w_s and w_i of signal and idler modes to be equal to w_p. The perfect thin-crystal regime is reached in the limit case $L/z_R \to 0$, which means for the focusing parameter $\overline{w}_p \to \infty$. Nevertheless, we can assume a good agreement between the thick- and thin-crystal regimes even for small values of the focusing parameter when one deals with small spatial subspaces in respect of p and ℓ (see Fig. 1). Furthermore, since the amplitudes of the thick (5) and thin (6)-crystal regimes depend only on $\overline{w}_p$, from Eq. (7) follows that the trace distance D is also uniquely determined by $\overline{w}_p$. This statement can be confirmed if the relation $w_p \propto \sqrt{\lambda_p L}$ applies for a fixed trace distance D [see Eq. (8)], which we will investigate next.

Figure 2 shows the trace distance D as a function of the crystal length L and the beam waist w_p for the typical wavelength $\lambda_p = 405$ nm. The thin-crystal approximation is *well* fulfilled in the white region (upper left quarter), whereas in the purple region (region under solid line), it is not justified. Any calculations in the purple area would lead to a deviation from the thin-crystal regime and strongly affect the spatial mode distribution of the two-photon state. Especially, spatially engineered high-dimensional, entangled states based on thin-crystal approximation will dramatically change if the approximation is not well satisfied. In principle, if the pump beam waist is large enough, a good fulfillment of the thin-crystal regime can be reached for any crystal length. Furthermore, we also indicated in Fig. 2 the curves with conditions $D = 0.1$ (dashed line) and $D = 0.5$ (solid line) to confirm the expected relation $w_p \propto \sqrt{L}$. As we can see, the smaller the selected trace distance D is, the larger the curve slope.

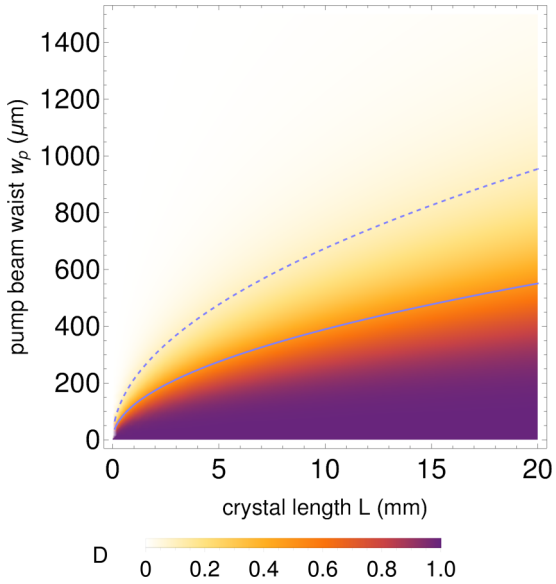

FIG. 2. Trace distance D as a function of crystal length L and pump beam waist w_p for the typical wavelength, $\lambda_p = 405$ nm. The white region (upper left quarter) refers to a well fulfillment of the thin-crystal approximation. In contrast, the purple region (region under solid line) indicates a strong violation of the approximation. The dashed and solid lines display the conditions $D = 0.1$ and $D = 0.5$, respectively. These curves show a square root dependence $w_p \propto \sqrt{L}$, where the higher D is, the larger the slope of the curve.

To consider also different wavelengths, we analyzed the trace distance as a function of the focusing parameter $\overline{w}_p$ (the dashed curve in Fig. 3). As we can see, the trace distance tends to one, $D \to 1$ if the focusing parameter tends to zero. In contrast, the trace distance tends to zero, $D \to 0$ if $\overline{w}_p \to \infty$. In order to reach a good fulfillment of the thin-crystal approximation (for the full state), very large values of the focusing parameter are required. On the other hand, most spatial correlation experiments are performed in small spatial mode subspaces, where the condition of reaching the thin-crystal regime will be less strict.

The solid curve in Fig. 3 represents the same as the dashed curve but for the subspace $p_{s,i} = 0,\ 1$ and $\ell_{s,i} = -2,\ -1,\ 0,\ 1,\ 2$ that was already presented in Fig. 1. As we could expect, for the same $\overline{w}_p$, the approximation is better satisfied for the subspace case. The reason for this behavior

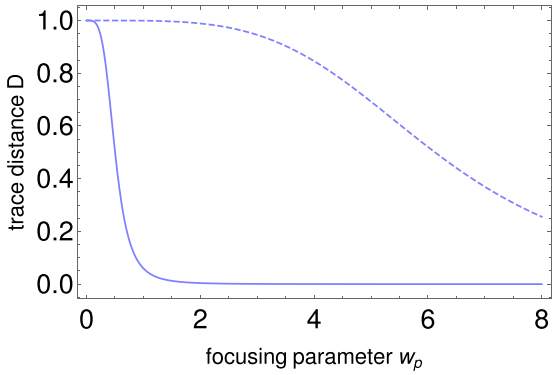

FIG. 3. The relation between the trace distance D and the focusing parameter $\overline{w}_p$ was calculated for the full state (dashed line) and the subspace $p_{s,i} = 0,\ 1$ and $\ell_{s,i} = -2,\ -1,\ 0,\ 1,\ 2$ (solid line). The efficiency of the thin-crystal approximation increases with $\overline{w}_p$. In contrast to the full state, the approximation is well fulfilled for relatively small focusing parameter values if small subspaces are considered.

is that the modes with higher mode numbers $2p + \ell$ diverge faster than the lower modes (see Fig. 1). In other words, the deviation between the same modes from the thick and thin-crystal regimes increases with the mode number.

The possible Poynting walk-off of the pump beam in the crystal has not been considered in our calculations. Torres *et al*. have shown that the Poynting walk-off can be neglected if $w_p \gg L$ [45]. Since we are more interested in the region $\overline{w}_p \gg 1$ or $w_p \gg L$, where the thin-crystal approximation is valid, the results for the determination of the thin-crystal regime should not be affected by a possible Poynting walk-off of the pump beam. The spatial walk-off can be neglected for periodically poled $KRiOPO_4$ (PPKTP) crystal even if $w_p \propto L$, but should be taken into account, for BBO crystal. In general, the spatial walk-off plays a role if the angle of the optical axis and the polarization of the pump is not neglectable.

In conclusion, we have explored the validity of the thin-crystal approximation in the SDPC process and find that fulfillment of this often-employed approximation can be determined for many experimental situations by just calculating $\overline{w}_p$ and comparing it either with Fig. 2 or Fig. 3. Our quantitative guideline will be helpful for experimentalists, in particular in high-dimensional quantum-information processing with spatially entangled photons as well as quantum and nonlinear imaging techniques based on SPDC [46].

[1] P. G. Kwiat, A. M. Steinberg, and R. Y. Chiao, Phys. Rev. A **47**, R2472 (1993).
[2] D. V. Strekalov, T. B. Pittman, A. V. Sergienko, Y. H. Shih, and P. G. Kwiat, Phys. Rev. A **54**, R1 (1996).
[3] I. A. Khan and J. C. Howell, Phys. Rev. A **73**, 031801(R) (2006).
[4] I. Ali-Khan, C. J. Broadbent, and J. C. Howell, Phys. Rev. Lett. **98**, 060503 (2007).
[5] P. G. Kwiat, E. Waks, A. G. White, I. Appelbaum, and P. H. Eberhard, Phys. Rev. A **60**, R773 (1999).
[6] P. G. Kwiat, K. Mattle, H. Weinfurter, A. Zeilinger, A. V. Sergienko, and Y. Shih, Phys. Rev. Lett. **75**, 4337 (1995).
[7] X.-L. Wang, L.-K. Chen, W. Li, H.-L. Huang, C. Liu, C. Chen, Y.-H. Luo, Z.-E. Su, D. Wu, Z.-D. Li, H. Lu, Y. Hu, X. Jiang, C.-Z. Peng, L. Li, N.-L. Liu, Y.-A. Chen, C.-Y. Lu, and J.-W. Pan, Phys. Rev. Lett. **117**, 210502 (2016).
[8] H.-S. Zhong, Y. Li, W. Li, L.-C. Peng, Z.-E. Su, Y. Hu, Y.-M. He, X. Ding, W. Zhang, H. Li, L. Zhang, Z. Wang, L. You, X.-L. Wang, X. Jiang, L. Li, Y.-A. Chen, N.-L. Liu, C.-Y. Lu, and J.-W. Pan, Phys. Rev. Lett. **121**, 250505 (2018).

[9] A. Rossi, G. Vallone, A. Chiuri, F. De Martini, and P. Mataloni, Phys. Rev. Lett. **102**, 153902 (2009).

[10] A. Mair, A. Vaziri, G. Weihs, and A. Zeilinger, Nature **412**, 313 (2001).

[11] M. Krenn, M. Huber, R. Fickler, R. Lapkiewicz, S. Ramelow, and A. Zeilinger, Proc. Natl. Acad. Sci. USA **111**, 6243 (2014).

[12] J. Leach, B. Jack, J. Romero, A. K. Jha, A. M. Yao, S. Franke-Arnold, D. G. Ireland, R. W. Boyd, S. M. Barnett, and M. J. Padgett, Science **329**, 662 (2010).

[13] A. Vaziri, G. Weihs, and A. Zeilinger, Phys. Rev. Lett. **89**, 240401 (2002).

[14] J. Romero, D. Giovannini, S. Franke-Arnold, S. M. Barnett, and M. J. Padgett, Phys. Rev. A **86**, 012334 (2012).

[15] R. W. Boyd, *Nonlinear Optics, Third Edition*, 3rd ed. (Academic Press, New York, 2008).

[16] T. E. Keller and M. H. Rubin, Phys. Rev. A **56**, 1534 (1997).

[17] C. Kurtsiefer, M. Oberparleiter, and H. Weinfurter, J. Mod. Opt. **48**, 1997 (2001).

[18] F. Steinlechner, M. Gilaberte, M. Jofre, T. Scheidl, J. P. Torres, V. Pruneri, and R. Ursin, J. Opt. Soc. Am. B **31**, 2068 (2014).

[19] C. K. Hong and L. Mandel, Phys. Rev. A **31**, 2409 (1985).

[20] B. E. A. Saleh, A. F. Abouraddy, A. V. Sergienko, and M. C. Teich, Phys. Rev. A **62**, 043816 (2000).

[21] S. Walborn, C. Monken, S. Pádua, and P. Souto Ribeiro, Phys. Rep. **495**, 87 (2010).

[22] G. Molina-Terriza, J. P. Torres, and L. Torner, Opt. Commun. **228**, 155 (2003).

[23] D. N. Nikogosyan, Appl. Phys. A **52**, 359 (1991).

[24] R.-B. Jin, M. Takeoka, U. Takagi, R. Shimizu, and M. Sasaki, Sci. Rep. **5**, 9333 (2015).

[25] F. M. Miatto, A. M. Yao, and S. M. Barnett, Phys. Rev. A **83**, 033816 (2011).

[26] C. H. Monken, P. H. Souto Ribeiro, and S. Pádua, Phys. Rev. A **57**, R2267 (1998).

[27] Y. Zhang, M. Mclaren, F. S. Roux, and A. Forbes, Opt. Express **22**, 17039 (2014).

[28] C. H. Monken, P. H. Souto Ribeiro, and S. Pádua, Phys. Rev. A **57**, 3123 (1998).

[29] M. McLaren, J. Romero, M. J. Padgett, F. S. Roux, and A. Forbes, Phys. Rev. A **88**, 033818 (2013).

[30] Y. Zhang, F. S. Roux, M. McLaren, and A. Forbes, Phys. Rev. A **89**, 043820 (2014).

[31] J. P. Torres, Y. Deyanova, L. Torner, and G. Molina-Terriza, Phys. Rev. A **67**, 052313 (2003).

[32] B. Baghdasaryan and S. Fritzsche, Phys. Rev. A **102**, 052412 (2020).

[33] S. Liu, Y. Zhang, C. Yang, S. Liu, Z. Ge, Y. Li, Y. Li, Z. Zhou, G. Guo, and B. Shi, Phys. Rev. A **101**, 052324 (2020).

[34] E. V. Kovlakov, S. S. Straupe, and S. P. Kulik, Phys. Rev. A **98**, 060301(R) (2018).

[35] S. Liu, Z. Zhou, S. Liu, Y. Li, Y. Li, C. Yang, Z. Xu, Z. Liu, G. Guo, and B. Shi, Phys. Rev. A **98**, 062316 (2018).

[36] R. Ramírez-Alarcón, H. Cruz-Ramírez, and A. B. U'Ren, Laser Phys. **23**, 055204 (2013).

[37] J. P. Torres, A. Alexandrescu, and L. Torner, Phys. Rev. A **68**, 050301(R) (2003).

[38] V. D. Salakhutdinov, E. R. Eliel, and W. Löffler, Phys. Rev. Lett. **108**, 173604 (2012).

[39] S. P. Walborn, A. N. de Oliveira, S. Pádua, and C. H. Monken, Phys. Rev. Lett. **90**, 143601 (2003).

[40] W. P. Grice, R. S. Bennink, D. S. Goodman, and A. T. Ryan, Phys. Rev. A **83**, 023810 (2011).

[41] G. Molina-Terriza, S. Minardi, Y. Deyanova, C. I. Osorio, M. Hendrych, and J. P. Torres, Phys. Rev. A **72**, 065802 (2005).

[42] A. M. Yao, New J. Phys. **13**, 053048 (2011).

[43] L. Allen, M. W. Beijersbergen, R. J. C. Spreeuw, and J. P. Woerdman, Phys. Rev. A **45**, 8185 (1992).

[44] M. A. Nielsen and I. L. Chuang, *Quantum Computation and Quantum Information* (Cambridge University Press, Cambridge, 2000).

[45] J. P. Torres, G. Molina-Terriza, and L. Torner, J. Opt. B: Quantum Semiclassical Opt. **7**, 235 (2005).

[46] M. Gilaberte Basset, F. Setzpfandt, F. Steinlechner, E. Beckert, T. Pertsch, and M. Gräfe, Laser Photonics Rev. **13**, 1900097 (2019).